Tennessee State University

Digital Scholarship @ Tennessee State University

Mechanical and Manufacturing Engineering Faculty Research

Department of Mechanical and Manufacturing Engineering

1-27-2021

Effect of Varying Wind Intensity, Forward Speed, and Surface Pressure on Storm Surges of Hurricane RitaEffect of Varying Wind Intensity, Forward Speed, and Surface Pressure on Storm Surges of Hurricane Rita

Abram Musinguzi
Tennessee State University

Muhammad K. Akbar
Tennessee State University

Follow this and additional works at: https://digitalscholarship.tnstate.edu/me-faculty

 Part of the Mechanical Engineering Commons, and the Oceanography and Atmospheric Sciences and Meteorology Commons

Recommended Citation

Musinguzi, A.; Akbar, M.K. Effect of Varying Wind Intensity, Forward Speed, and Surface Pressure on Storm Surges of Hurricane Rita. J. Mar. Sci. Eng. 2021, 9, 128. https://doi.org/10.3390/jmse9020128

This Article is brought to you for free and open access by the Department of Mechanical and Manufacturing Engineering at Digital Scholarship @ Tennessee State University. It has been accepted for inclusion in Mechanical and Manufacturing Engineering Faculty Research by an authorized administrator of Digital Scholarship @ Tennessee State University. For more information, please contact XGE@Tnstate.edu.

Journal of *Marine Science and Engineering*

MDPI

Article

Effect of Varying Wind Intensity, Forward Speed, and Surface Pressure on Storm Surges of Hurricane Rita

Abram Musinguzi [1] and Muhammad K. Akbar [2,*]

[1] Department of Civil and Architectural Engineering, Tennessee State University, Nashville, TN 37209, USA; amusingu@my.tnstate.edu
[2] Department of Mechanical and Manufacturing Engineering, Tennessee State University, Nashville, TN 37209, USA
* Correspondence: makbar@tnstate.edu; Tel.: +1-615-963-5392

Abstract: Hurricane storm surges are influenced by several factors, including wind intensity, surface pressure, forward speed, size, angle of approach, ocean bottom depth and slope, shape and geographical features of the coastline. The relative influence of each factor may be amplified or abated by other factors that are acting at the time of the hurricane's approach to the land. To understand the individual and combined influence of wind intensity, surface pressure and forward speed, a numerical experiment is conducted using Advanced CIRCulation + Simulating Waves Nearshore (ADCIRC + SWAN) by performing hindcasts of Hurricane Rita storm surges. The wind field generated by Ocean Weather Inc. (OWI) is used as the base meteorological forcing in ADCIRC + SWAN. All parameters are varied by certain percentages from those in the OWI wind field. Simulation results are analyzed for maximum wind intensity, wind vector pattern, minimum surface pressure, forward speed, maximum water elevation, station water elevation time series, and high water marks. The results for different cases are compared against each other, as well as with observed data. Changes in the wind intensity have the greatest impact, followed by the forward speed and surface pressure. The combined effects of the wind intensity and forward speed are noticeably different than their individual effects.

Keywords: storm surge hindcast; wind intensity; forward speed; surface pressure and wide and gentle sloping continental shelf

check for updates

Citation: Musinguzi, A.; Akbar, M.K. Effect of Varying Wind Intensity, Forward Speed, and Surface Pressure on Storm Surges of Hurricane Rita. *J. Mar. Sci. Eng.* **2021**, *9*, 128. https://doi.org/10.3390/jmse9020128

Academic Editor: Efim Pelinovsky
Received: 9 January 2021
Accepted: 20 January 2021
Published: 27 January 2021

Publisher's Note: MDPI stays neutral with regard to jurisdictional claims in published maps and institutional affiliations.

Copyright: © 2021 by the authors. Licensee MDPI, Basel, Switzerland. This article is an open access article distributed under the terms and conditions of the Creative Commons Attribution (CC BY) license (https://creativecommons.org/licenses/by/4.0/).

1. Introduction

Extreme hurricanes winds are among the major destructive forces that may cause severe storm surges and inland flooding at landfall. A hurricane generates in the deep ocean, lashes towards the coast, and then propagates over the continental shelf, where it interacts with coastal features, ocean bathymetry, tides, currents and waves. Rapid changes in ocean currents, tides, and waves in the shallow coastal areas bring about storm surges. A hurricane experiences changes that span a wide range of spatial and temporal scales. These multiscale physical processes of hurricanes influence the generation and propagation of storm surges. The timing of the storm may heavily influence both storm surges and tides, either intensifying or weakening them [1–4].

National Hurricane Center (NHC) lists several factors that influence a storm surge, including storm intensity, size, surface pressure, forward speed, track and angle of approach, landfall location and bathymetry [5]. Conventionally, higher intensity winds, rotating counterclockwise, act on the right side of the storm generated on the northern hemisphere. Forward speed is the motion of the storm that may contribute positively or negatively to the wind intensity. When hurricane winds and forward speed move in the same direction, the forward speed intensifies the wind. This additive effect may increase storm surges on the right side of the hurricane. The reverse happens when the storm moves opposite to hurricane winds; this happens on the left side of hurricanes approaching US coasts over the Gulf of Mexico [6].

Hurricane structures and geographical features can be significantly different from hurricane to hurricane, as evident in most recent hurricanes, such as Harvey (2017), Irma (2017), and Dorian (2019). The radial structure of a hurricane is important in the sensitivity of wind and storm surge hazards [7,8]. How and why these structural and geographical features impact a hurricane storm surge is still not well understood.

The slope, size, and geographical features of a continental shelf play a critical role in hurricane storm surges. For example, Hurricane Ike (2008) produced a high water level surge, called a forerunner, in western Louisiana and Texas (LATEX) coasts about 12–24 h in advance of landfall [9–11]. In some places, the water level was as high as 3 m, although the cyclonic wind was primarily shore parallel. The authors [9] pointed out that a similar event happened during the 1900 and 1905 Galveston Hurricanes, although to a lesser extent. This unpredicted surge anomaly is explained through the phenomenon of Ekman setup, which is caused by a gradually sloped wide and shallow coastal shelf subject to large wind fields and the Coriolis effect.

The hurricane size, slope, and angle of approach have been studied for peak surges. A pioneer study [12] attempted to quantify the relationship between storm size and peak surge size for different bottom slopes by using idealized synthetic hurricanes using the ADvanced CIRCulation (ADCIRC) [13–15] storm surge model. The study shows that as the storm size increased, surge peak increased as well. The effect of size became more pronounced when the bottom slope was reduced. The sensitivity of impact of hurricane track, more specifically angle of approach, on peak surge was studied as well. For mildly sloped bottoms, a more negative or easterly angle of approach produced higher surges than the due north tracks. The analysis further showed that increased forward speed produced higher surges for steep to moderate bottom slopes but had little effect on mild slopes.

A numerical investigation of storm surge along the coast of Louisiana was conducted to understand the impact of forward speed on storm surges [16]. The Finite-Volume Coastal Ocean Model (FVCOM) was used to simulate Hurricane Rita and validated against in situ measurements. Experiments were done with different parameters to evaluate their impacts on inundation over a wide and shallow shelf of LATEXT. It was concluded that a faster hurricane along the LATEXT shelf produces higher surges, but smaller total flooded volumes. In a follow-up study [17] by the same authors, it was concluded that wind field asymmetry has a significant impact both on the peak and volume of the surge.

The impact of hurricane landfall location, direction and speed of approach, and intensity on storm surges was studied for Tampa Bay using a finite volume coastal model [18]. It was concluded that a hurricane approaching slowly towards coastline produces a larger surge in a semi-closed bay. The reason for this is that the translational time scale is larger than the storm surge set up or re-distribution time scale. The scenario can be worse when a hurricane makes landfall at the north of the bay with maximum wind at the mouth of the bay.

Most recently, Thomas et al. [19] have studied the effects of storm timing and forward speed on tides and storm surges for Hurricane Matthew, which was a shore-parallel storm. They found that observation-based wind fields provided better meteorological forcing for hindcasting than those from parametric models. The timing of the storm may have caused an increased or decreased water level due to the nonlinear relationship between storm surge and tide. The forward speed of the storm had large effects on water levels. Slower storms caused more flooding in bays and estuaries and less flooding in open coast. The opposite effects were noticed for faster storms. Another study [16] found that increasing forward speed increased peak surge heights but decreased inland volume of flood during hurricane Rita, and that varying forward speed can have a significant impact on flooded volumes, equivalent to an upgrade or downgrade of about 1- Category on the Saffir Simpson Scale.

The effects of storm surge and flooding tend to become more dangerous when winds act on a wide and gentle sloping continental shelf [20]. Shallower bathymetric depths intensify the wind-driven component of storm surge, hence making wind stress a critical factor in extensive regions of shallow water where water depth is low [16]. Water surface

elevations during hurricane Ike in Galveston Bay were dominated by the counterclockwise hurricane winds and that increasing wind speeds by 15% results in an approximately 23% higher surge [21]. In contrast, storm surge effects can be significantly different in narrow and deep ocean islands where the storm surge is produced mainly by changes in surface pressures due to the inverted barometer effect [22]. The lack of broad shelf to dissipate wave energy can result in large waves, and the presence of deep bathymetry tends to limit the wind-driven component of the storm surge in the coastal zones of deep ocean islands [23]. Hurricane pressure deficit was the main contributor to storm surges around Puerto Rico and the US Virgin Islands, an area which is characterized by adjacent deep ocean water and narrow continental shelves [24].

Although there have been several studies to quantify the impact of hurricane structure, forward speed, angle of approach, track, landfall features, etc., as potential influencers of the storm surge, every hurricane is different and a generalized knowledge base on the topic does not exist. The goal of this case study is to minimize the knowledge gap by understanding the effect of wind intensity, forward speed and surface pressure on storms acting over a wide and gentle sloping ocean coast, specifically by examining the Unites States coast on the Gulf of Mexico, a region that was intensely impacted by hurricane Rita in 2005. The wind intensity, forward speed and surface pressure are systematically decreased and increased to understand their individual effects, as well as combined effects. To the best of our knowledge, this study is the first to study the combined effects of wind intensity and forward speed on storm surge. Authors previously studied the effect of bottom friction, wind drag coefficient, and meteorological forcing on hurricane Rita storm surge [25]. In a subsequent study [26], the effect of meteorological forcing from forecasted, parametric models, and Ocean Weather Inc. (OWI) model were performed. The current study can be considered as a follow-up study to these.

2. Region of Study

The warm waters of the Gulf of Mexico and the western Caribbean Sea provide an abundant energy source for intense storms during the Atlantic basin hurricane season, which typically runs from May to November [27]. The Gulf of Mexico has experienced high occurrences of intense historical storms, such as Charley, Frances, and Ivan (2004); Katrina and Rita (2005); Gustav and Ike (2008); Isaac and Sandy (2012); Harvey (2017); and most recently Laura (2020).

Hurricane Rita is among the most powerful storms to ever hit the southern coastal areas of Louisiana and Texas. The storm intensified from tropical storm to category 5 hurricane in less than 36 h. It then maintained a category 5 for the next 18 h, reaching its estimated peak intensity of 178 mph by 0300 UTC 22 September. Rita then abruptly weakened to category 4, and further weakened by next day to category 3 after slightly increasing in forward speed from 4 to 5 m/s. Rita maintained Category 3 status until landfall in southwestern Louisiana just west of Johnson's Bayou and just east of Sabine Pass at 0740 UTC 24 September [28]. Hurricane Rita made a landfall at category 3 with an estimated intensity of 115 mph, a barometric pressure of 937 mbar and forward speed of about 5 m/s [28].

The Unstructured ULtralite-Levee-Removed (ULLR) [29] mesh is displayed in Figure 1a. The region of interest has a wide and gently sloping continental shelf, as shown in Figure 1b. The contour map of bathymetric depth shows many coastal communities on the gulf coast, including some areas located up to several miles inland from the coastline, lie within 1.5 m (see the black line in Figure 1b) below sea level. This renders these areas vulnerable to storm surges, since the ocean floor gradually deepens offshore. There are other complex features such levees, barrier islands, tidal marshes, estuaries and rivers that heavily impact the behavior of surges [29].

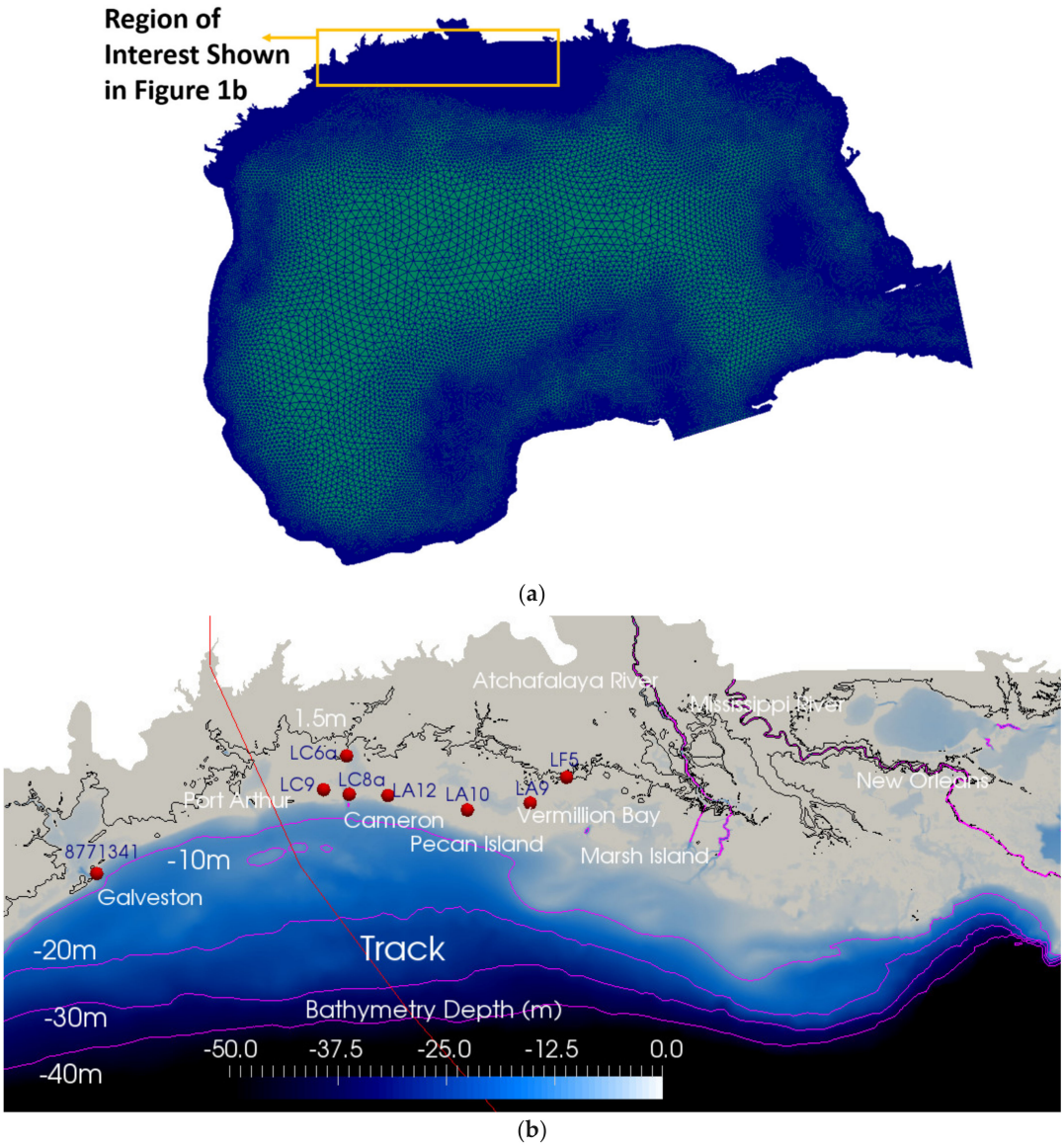

Figure 1. Unstructured ULtralite-Levee-Removed (ULLR) [29] mesh (**a**) domain and mesh; (**b**) observation station locations with respect to Hurricane Rita track indicated by red dots. Note that the negative bathymetry represents below sea level.

3. Methodology

3.1. Mesh and Hydrodynamic Model

This study uses the ULtralite- Levee-Removed (ULLR), unstructured triangular mesh with 417,642 nodes and 826,866 elements. The mesh covers the entire Gulf of Mexico, which stretches approximately 1600 km west-east and 900 km north-south. The mesh was created by [29], during the U.S. IOOS Coastal and Ocean Modeling Testbeds. The mesh covers the entire Gulf of Mexico and has open ocean boundaries at the Straits of Florida and Yucatan channel, and extends across the entire low-lying floodplains of Texas and Louisiana. Although not used in the present study, the mesh has river flux boundary conditions at its domain intersections with the Atchafalaya and Mississippi Rivers [29]. The principal tidal constituents were generated from the EC2001 tidal database [30]. More details are available in Kerr et al. [29]. ULLR resolution is coarser in the Gulf and finer inland, with a higher resolution needed to resolve key geographical features. The ULLR mesh's resolution ranges from 8 to 30 km in the Gulf, 2 to 8 km on the shelf, 500 to 2000 m on the floodplain, and 100 to 500 m in the rivers. Model details can be found in [29].

The ADCIRC and Simulating Waves Nearshore (ADCIRC+SWAN) is a tightly coupled model used to simulate waves and storms. ADCIRC uses the continuous-Galerkin finite element method to solve shallow-water equations to model hurricane storm surges on unstructured meshes [13,14]. The wind drag formulation of Powell with a cap of 0.002 is adopted in this study, as was done in previous studies [25,26]. A spatially varying Manning's n bottom friction, the same as in Kerr et al. [29], is used in the present study. The SWAN model is a third-generation wave model [31] which is tightly coupled with ADCIRC to produce random, short-crested wind-generated waves on top of storm surges. The SWAN + ADCIRC model takes atmospheric pressure and horizontal wind velocity to compute water surface elevation, depth-integrated velocity, significant wave height and wave period.

3.2. Meteorological Forcing

ADCIRC requires the specification of a meteorological input file with wind velocity and atmospheric pressure fields. Configuration of parameters of wind intensity and surface pressure fields are modified by increasing or decreasing the multiplier in the meteorological input file. The time increment of the meteorological forcing is specified through meteorological wind time interval. This parameter can be controlled in the model parameter and periodic boundary condition file to vary the forward speed of the storm. Details of these files can be found in ADCIRC documentation [32].

The Interactive Objective Kinematic Analysis (IOKA) by Ocean weather Inc. (OWI), a data-assimilated wind model for the meteorological forcing, is used in the present study. In this model, wind and surface pressure fields are generated based on observations from anemometers, airborne and land-based Doppler radar, microwave radiometers, buoys, ships, aircraft, coastal stations and satellite measurements [33,34]. Studies [25,26] found OWI wind and pressure fields to be the best for hurricane Rita hindcast based on error statistics and correlation coefficient. Similarly, the OWI is found to be a reasonably good representation of the atmospheric forcing for hurricane Matthew and matched well with the observed time series of surface pressures and wind speeds [19]. Therefore, the OWI wind field is considered as the reference or base meteorological forcing for Hurricane Rita in the present study.

3.3. Numerical Experimentation

A total of 11 cases are simulated, in which three parameters are varied: (1) wind intensity, (2) forward speed and (3) surface pressure for the numerical experimentation. Table 1 shows the summary of experimental runs performed. Case 1 is the base case with original values, i.e., 100% intensity, 100% forward speed and 100% pressure of OWI meteorological data, are used. In Cases 2–7, each of the three parameters is decreased or increased one at a time. Wind intensity and forward speed are varied in increments of 25%, while the surface pressure is varied in 3.2% increments. In Cases 8–11, both wind intensity and forward speed are simultaneously changed to examine the combined effects of wind intensity and forward speed on hindcasted surge. Since the effect of surface pressure alone is found to be relatively small, it is not considered in the analysis of combined effects.

Wind intensity and forward speed manipulation are done through input files. For wind intensity experiment, the "Wind Velocity Multiplier" in the "fort.22", a meteorological input file native to ADCIRC, is changed. For the base model (Case 1) a velocity multiplier of 1.0 is used as the benchmark value (i.e., 100%). To achieve 75% and 125% of that wind intensity, multipliers are set to 0.75 and 1.25, respectively. For forward speed experiment, the meteorological "Wind Time Increment" parameter in "fort.15", the model parameter and periodic boundary condition file native to ADCIRC, is changed. In previous studies [25,26], the default value used for OWI used is 900 s. To achieve 75% and 125% of that forward speed, the wind time increment parameter is changed to 1200 and 720, respectively. The time step size is 4s, which means consecutive wind files are spaced at 0.8, 1 and 1.33 h for Case 4, Case 1 and Case 5, respectively. Notice that the time increments are not equal

for these cases, which causes the hurricane minimum pressure dips to space unequally, as discussed in the next paragraph.

Table 1. Parametric combinations used for different cases.

Case	Parameters		
	Wind Intensity	Forward Speed	Surface Pressure
1 (Base or OWI)	100%	100%	100%
2	75%	100%	100%
3	125%	100%	100%
4	100%	75%	100%
5	100%	125%	100%
6	100%	100%	96.8%
7	100%	100%	103.2%
8	75%	75%	100%
9	125%	125%	100%
10	75%	125%	100%
11	125%	75%	100%

Since the center pressure of a hurricane is the lowest in the entire domain at a given time, locations and times of the center pressures can be easily extracted from the atmospheric pressure time series output file of ADCIRC + SWAN. From that information, forward speeds of the hurricane can be calculated using intermediate distances and times hurricane needed to travel those distances. Figure 2 shows the pressure variations with date and time for Cases 1, 4 and 5. From the comparison between Case 4 and Case 1, it is evident that hurricane travels slower as the forward speed decreases. When forward speed is reduced (Case 4), the lowest minimum pressure (about 900 mBar) occurs approximately 36 h later than that of the base model (Case 1).

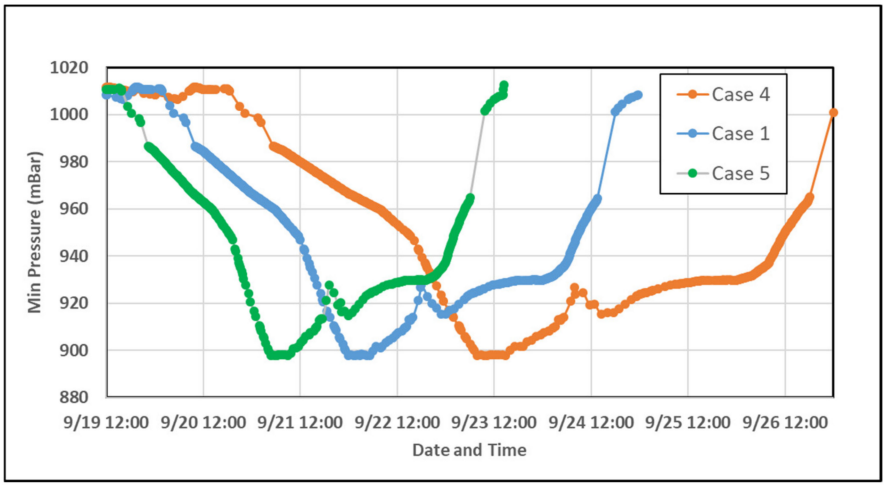

Figure 2. Effect of modified forward speed on center pressure with time.

The opposite is true when the forward speed increases (Case 5), although the lowest pressure arrives about 20 h earlier than that of Case 1. This is not shown here for brevity, but the average forward speed is highly transient throughout the hurricane life, and may vary from near zero to 30 m/s.

For the pressure experiment, initially, OWI surface pressures were multiplied by a factor of 0.975 and 1.025 to achieve 97.5% and 102.5% pressure. The resulting high pressures for the 102.5% case are capped down to atmospheric pressure, 1013 millibars. The ADCIRC routine "owiwind.f" was changed by adding a FORTRAN statement with the multiplication operation. However, it is understood from initial results that a linear change

in surface pressure does not impact storm surge much. The Shallow Water Equations used in storm surge modeling depend on a pressure gradient, not the pressure. A linear change in pressure does not change the pressure gradient much. Therefore, an alternative and more realistic pressure change is performed using the rectangular hyperbola distribution proposed by Holland et al. [35,36], as follows

$$P(r) = P_c + (P_n - P_c)e^{-(R_{max}/r)^B} \quad (1)$$

$$B = V_{max}^2 \rho e/(P_n - P_c) \quad (2)$$

Here, the maximum wind velocity, V_{max}, occurs at a distance R_{max}, $P(r)$ is the surface pressure at a distance r from the center, P_c is center pressure, P_n is the far-field pressure (assumed 1013 mBar), ρ is the air density (assumed 1.08 kg/m^3) and e is the base of natural logarithm. Hurricane parameters reported approximately 12 h before the landfall are adopted as reference values for this study. At that time (23 September, 6 p.m. UTC) R_{max} = 20 knots, V_{max} = 110 kn, P_c = 930 mBar. Two P_c values are chosen: P_c = 900 mBar (96.8% decrease) and P_c = 960 mBar (103.2% increase) for this experimentation. Pressure distribution with radial distance r, calculated using Equation (1) and plotted against that of reference P_c = 930 mBar. Third-order polynomial equations are used to modify the OWI surface pressure fields for Cases 6 and 7. Calculated pressure distributions are displayed in blue dots and polynomial trendlines are displayed in red lines in Figure 3.

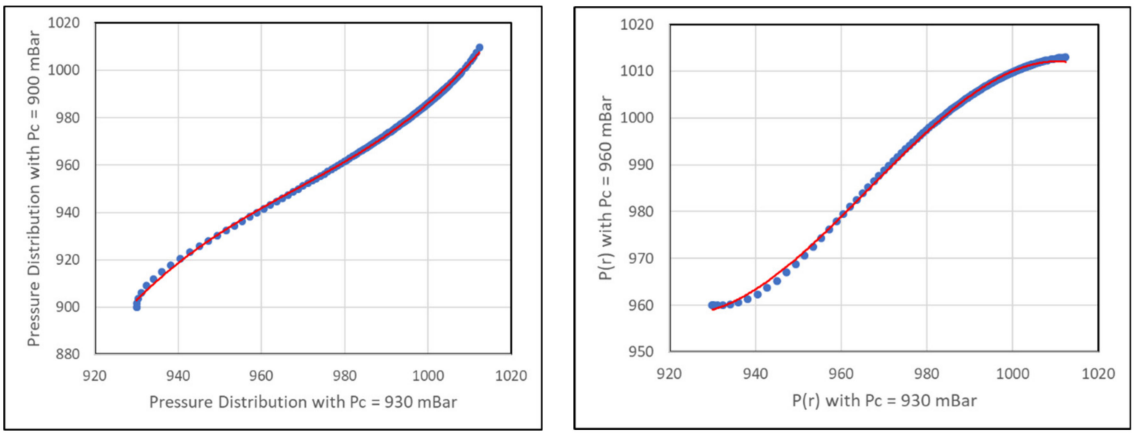

(**a**) (**b**)

Figure 3. Radial pressure $P(r)$ distribution (blue dots) with different center pressures, (**a**) Pc = 900 mBar vs Pc = 930 mBar, and (**b**) Pc = 960 mBar vs Pc = 930 mBar. Trendlines are displayed in red.

Each simulation is cold-started on 0000 UTC 13 August 2005, with a 36-day tides-only period that allows the tides to reach a dynamic equilibrium. This is followed by a 7.2-day Rita simulation from 0000 UTC 18 September 2005 to 0500 UTC 26 September 2005.

3.4. Model Validation

Error Statistics

The agreement between modeled and observed water levels is quantified using three statistical performance indicators: Coefficient of Determination (R^2); Mean Normalized Bias (B_{MN}) and Root Mean Square Error (E_{RMS}). Coefficient of Determination (R^2) describes how well a regression line fits a set of data, and has an ideal value of one. Mean Normalized Bias (B_{MN}) indicates the model's magnitude of overprediction or underprediction normalized to the observed value, with an ideal value of zero, and is expressed as

$$B_{MN} = \frac{\frac{1}{N}\sum_{i=1}^{N} E_i}{\frac{1}{N}\sum_{i}^{N}|O_i|} \quad (3)$$

Root Mean Square Error (E_{RMS}) is an indication of the magnitude of error, with an ideal value of zero; and can be expressed as

$$E_{RMS} = \frac{1}{N}\sum_{i=1}^{N} {E_i}^2 \quad (4)$$

where O is the observed value, E is the error in terms of simulated minus observed and N is the number of datapoints.

In previous studies, such as [19,29], the above statistics were used to validate model performance by utilizing only the wet stations or points, which is called the wet-only method. Kerr et al. [29] proposed another method of replacing dry points with the bathymetry as the common equalizer, which may overcome the problem of poor statistical performance when comparing multiple models. This method is called Topo-Substitution (TS). Since the bathymetry represents the minimum water level obtainable at any point in the mesh, dry values can be replaced with the ground surface elevation. SWAN + ADCIRC performed with a coefficient of determination value of 0.622 using Topo-Substitution and 0.663 using the wet-only method. They suggested that it is appropriate to use the wet-only method for a single model validation [29]. In this study, the statistical analyses of HWMs, used only wet locations predicted by simulations. The HWM points are distributed in Louisiana and Texas coasts, but most of the points are in Louisiana, on the east side of Rita's landfall location.

4. Results and Discussion

4.1. Evolution of Maximum Wind and Water Level

In Figure 4, the contour plots of Cases 2, 1 and 3 show the effect of increasing wind intensity on maximum wind velocity magnitude and maximum water elevation of storm surges that happen at every mesh node over the entire duration of hurricane. From relative sizes of red patches and relative distances of 1 m surge contour lines from the blue coast line in Figure 4b,d,f, it is obvious that storm surges increase with the wind intensity. However, it should be emphasized that as the wind intensity increases, the storm size also increases inadvertently, which can be inferred from the relative distance of contour line 30 m/s (or 15 m/s) from the track in Figure 4a,c,e. The storm surge increase is due to the combined effects of wind intensity and storm size. Similar findings for Rita hindcast studies were reported by Rego et al. [16] and Irish et al. [12]. They argued the effect of varying wind intensity on a storm surge is similar in magnitude to that of varying the radius of maximum wind along the coast of Louisiana.

The wind intensity and its impact on storm surge is further demonstrated by snapshots of wind velocity vectors and velocity magnitude color plots at the landfall time, as shown in Figure 5. Hurricane Rita made landfall approximately at 7:40 AM UTC on 24 September 2005, which corresponds to Case 1. All cases have the same landfall time as that of Case 1, unless forward speeds are changed (e.g., Cases 4, 5, 8–11). Asymmetric and anticlockwise rotating wind with stronger right-side patterns are obvious from all snapshots. Effect of the hurricane extends up to the blue background. It can be clearly seen from comparison between Figure 5a,b how increasing the wind intensity increases the storm size, as mentioned earlier. Figure 5c,d corresponds to Cases 4 and 5 with reduced and increased forward speeds. Although wind intensity patterns are similar to that of Case 1, as expected, landfall timings change with the forward speed. The landfalls of Case 4 and Case 5 happen at 1:00 a.m. on 23 September and 09:00 a.m. on 26 September, respectively.

To study the quantitative contrast of maximum water elevation between different cases, each case results are subtracted from those of Case 1. Color plots of these algebraic difference are shown in Figure 6. Note that the blue color represents the minuend (Case 1) water elevation being smaller than that in the subtrahend. Decreasing wind intensity by 25% (Case 2) decreases surge levels nearshore on the right sector of the storm by more than 1 m, as seen in Figure 6a. Weaker winds decrease overland flooding by 0.25 m to 1 m in

inland, bays, lakes and rivers. The surge decrease is visible in Sabine Lake, Calcasiue Lake, Vermallion Bay, Lake Pontchartrain, and in the mouths of Atchafalaya and Mississippi rivers. On the contrary, when the wind intensity is increased (Case 3), a more than 1 m increase in surge is observed nearshore, as seen in Figure 6b. Stronger winds push water overland, and the surge increases by 0.25 to 1 m in inlands, bays, lakes, and rivers.

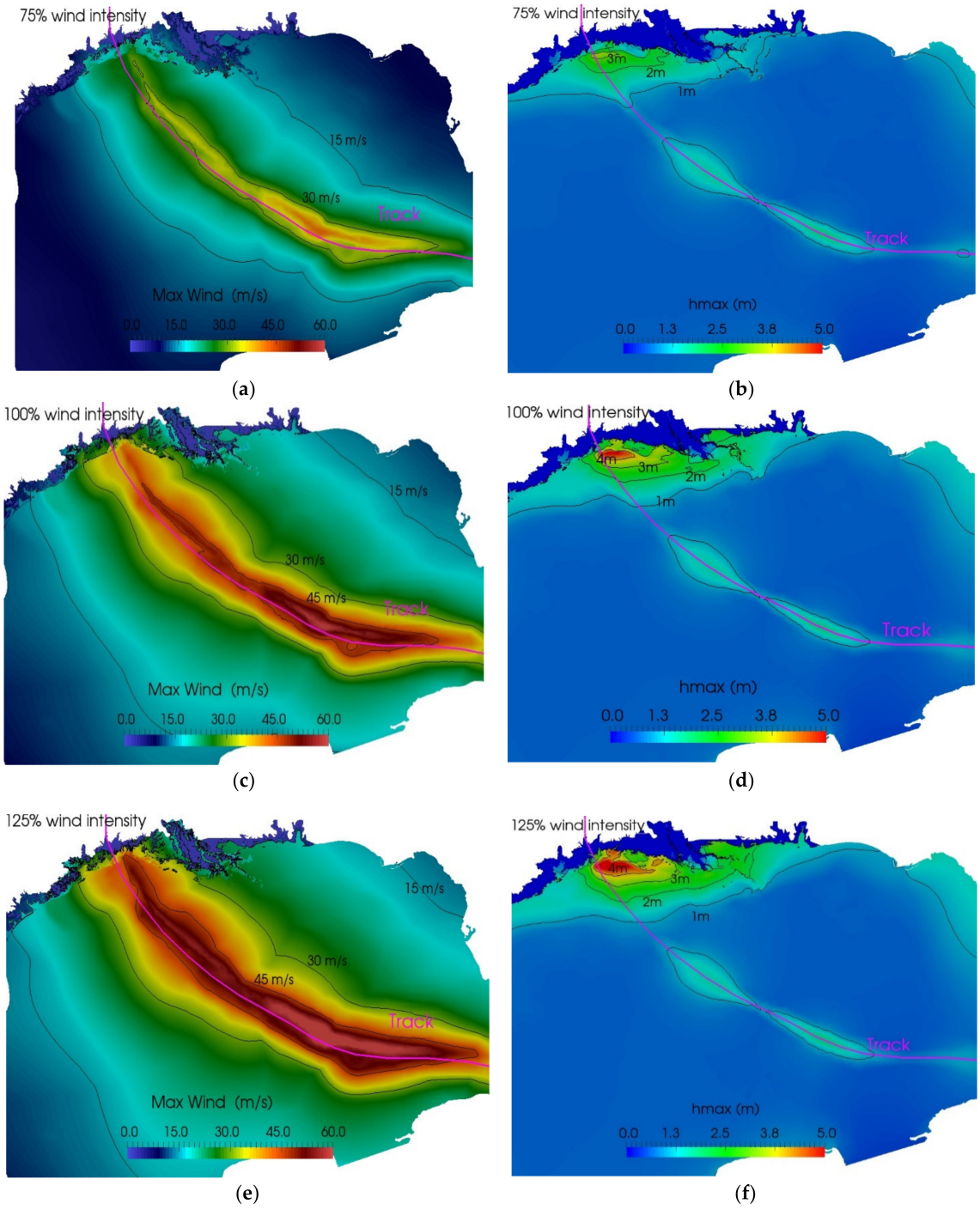

Figure 4. Effect of wind intensity on maximum wind velocity magnitude and maximum water elevation; (**a**) and (**b**) Case 2, (**c**) and (**d**) Case 1, and (**e**) and (**f**) Case 3. Left column: maximum wind velocity magnitude; right column: maximum water elevations. Relevant contour lines are displayed in each figure.

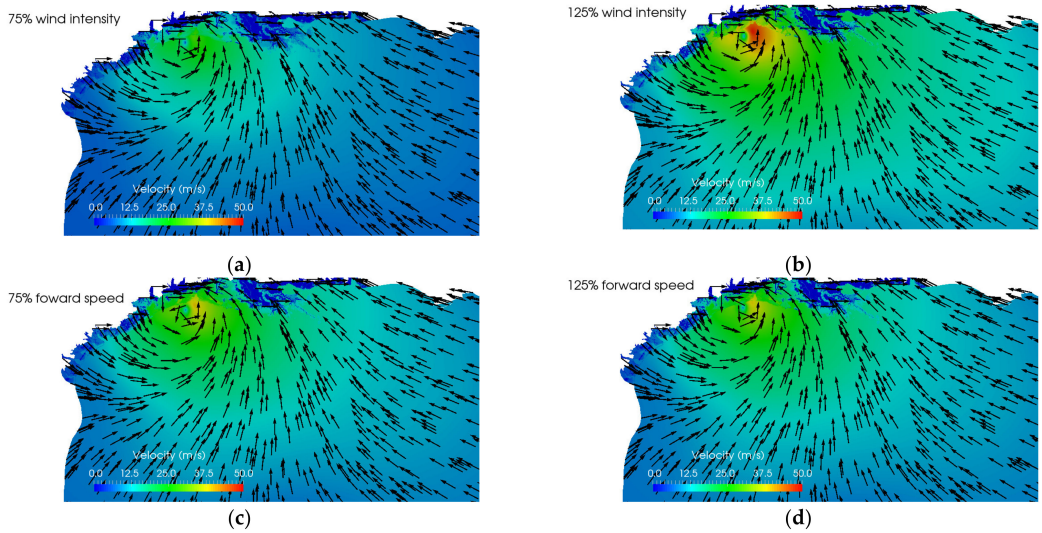

Figure 5. Snapshots of wind vector and velocity magnitude color plots at landfall for different meteorological forcings, (**a**) Case 2, (**b**) Case 3, (**c**) Case 4, and (**d**) Case 5.

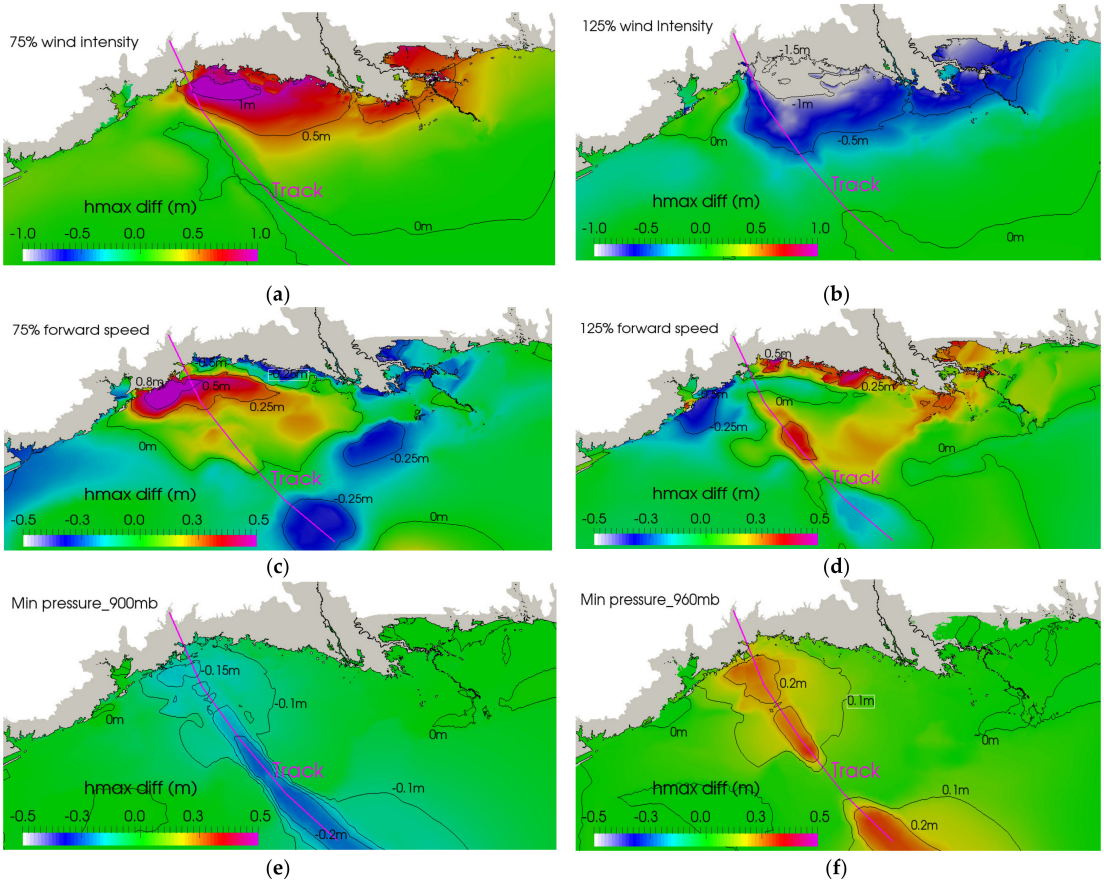

Figure 6. Departure of maximum water elevations from the base case (i.e., "hmax" of each simulation is subtracted from that of the base simulation); (**a**) Case 1–Case 2; (**b**) Case 1–Case 3; (**c**) Case 1–Case 4; (**d**) Case 1–Case 5; (**e**) Case 1–Case 6; and (**f**) Case 1–Case 7. Purple lines represent the Rita track.

A reduction in the hurricane forward speed by 25% (Case 4) decreases flooding in the nearshore, as seen in Figure 6c. However, a slow-moving storm provides more time for water to push overland, which causes a 0.25 to 0.5 m higher surge in the inland, bays,

lakes and rivers. A slower forward speed causes a high surge in the Galveston bay area, located on the west side of Rita landfall. Interestingly, a slower and faster moving hurricane may cause localized higher and lower water elevations in the deep ocean, displayed as blue blotches in Figure 6c and red blotches in Figure 6d, respectively. The exact reason of these blotches is not known, but these may have resulted from the additive or subtractive combined effect of the forward speed and wind velocity components at those locations. A slower hurricane, causing an increased inland surge, was reported by Thomas et al. [19] for Hurricane Matthew. When forward speed is increased by 25% (Case 5), an opposite effect is noticed (see Figure 6d)—increased flooding nearshore, but a 0.25 to 0.5 m decreased surge in inland lakes, bays and rivers. A decreased surge also occurs in the Galveston area, although the surrounding nearshore ocean has a higher surge.

Changes in wind pressure are found to have a relatively smaller effect on the storm surge. As shown in Figure 6e, a decrease in pressure (Case 6) results in about a 0.2 m surge increase due to the inverted barometer effect. The increase in the surge is mainly along the track, mostly in the deeper water away from the coastline. When the pressure is increases (Case 7), there is about a 0.2m reduction in surge levels on the nearshore, as seen in Figure 6f. According to a classical theoretical relation [37], water rise of 1 cm results from every millibar of pressure drop, provided that (1) the pressure change is not too rapid, and (2) water can freely flow to the low-pressure regions. A free flow of water is expected in the open ocean or coast where water is not too shallow. Moreover, a changed pressure is expected to influence the wind field, since these parameters are coupled and correlated [37]. In agreement with this theoretical relation, Joyce et al. [24] found surge levels to rise by 0.8 to 1 m around Puerto Rico and the U.S. Virgin Islands for Hurricanes Irma and Maria, with center pressures of 914 and 910 millibar, respectively. Surge level increasing or decreasing by 0.2 m for a 30 millibar incremental pressure drop or rise in the present study is within 67% of the classical theoretical relation mentioned above. Possible reasons for not obtaining better accuracy are (1) decoupled wind field from the modified pressure used in the study, and (2) the gently slopped continental shelves with shallow waters near and around Hurricane Rita landfall.

4.2. Analysis of Surge Time Series

Table 2 displays site information of water-level observation stations used in the study, all deployed in south Louisiana and Texas during Hurricane Rita. The geographic locations of these stations with respect to the track are shown in Figure 1. Most of the stations belong to the U.S. Geological Survey (USGS). All selected USGS stations are located on the east of landfall. In order to study the effect of storm on the west side of landfall, one station operated by the National Oceanic and Atmospheric Administration (NOAA) was selected on the Galveston Bay Entrance, North Jetty, TX (Station ID 8771341). Maximum water elevations listed in Table 2 are all in reference to the North American Vertical Datum of 1988 (NAVD 88). A review of the observed data indicates that the highest water levels were recorded during the early morning of September 24 on nearshore stations. Maximum recorded water levels for stations further inland occurred several hours later after the landfall, and were generally lower than the nearshore stations. Among the selected stations, the highest water elevation was 4.52 m above NAVD 88 near Creole, LA (Station LA12), located 48 miles east of Sabine Pass, Texas. The lowest maximum water level was recorded at Galveston Bay Entrance.

The ADCIRC + SWAN water level time series for different simulation cases are compared with the observed water levels at eight stations in Figure 7. A detailed discussion of these stations, their geographical locations, and possible reasons for high or low water surges are provided in Kerr et al. [29]. The current discussion relies on the findings of that study. For all stations on the east of the landfall, increasing wind intensity by 25% increases the peak water levels with respect to the base model, Case 1. Surge overpredictions are higher for inland stations than for stations closer to the open coast. The highest overprediction of about 2.5 m occurs at the inland station LC6a (see Figure 7e) for Case 3.

Peak surge for inland stations occurs slightly earlier than the peaks for the observed data. The station is located farther inland with a network of channels, which might have contributed to the exceptional surge behavior. For the station on the west side of the track, no significant surge difference is visible, indicating that the surge there is not a direct effect of the storm, but rather an after effect. When wind intensity is decreased by 25% (Case 2), peak water levels for all stations on the east side of track are decreased. It is important to note that for Case 2, the model generally underpredicts the surge, except for an inland station LC6a, in which peak surge levels are overpredicted by 0.5 m with respect to the observed data. The peak surge for inland stations occurs slightly earlier than the peak surge for the observed data. The surge for the west side station remains mostly unchanged again.

Table 2. Information about United States Geological Survey (USGS) Deployed (DEPL) and National Oceanic and Atmospheric Administration (NOAA) observation stations used in present study.

Station ID	Longitude (°)	Latitude (°)	Max Recorded Water Elevation (m)	Date and Time of Peak Water Level
USGS-DEPL LA10 (Nearshore)	−92.67552	29.70658	2.65	9/24/05 04:26:14
USGS-DEPL LA12 (Nearshore)	−93.11494	29.7861	4.52	9/24/05 01:57:20
USGS-DEPL LA9 (Inland)	−92.32792	29.74476	2.02	9/24/05 10:52:58
USGS-DEPL LC6a (Inland)	−93.34333	30.00432	1.54	9/24/05 09:26:44
USGS-DEPL LC8a (Nearshore)	−93.32886	29.79764	4.07	9/24/05 02:09:57
USGS-DEPL LC9 (Nearshore)	−93.47052	29.81823	4.21	9/24/05 02:28:55
USGS-DEPL LF5 (Inland)	−92.12703	29.88604	3.07	9/24/05 08:48:26
NOAA 8771341 (Nearshore)	−94.7250	29.3567	0.94	9/25/05 7:24:00

When the forward speed is increased by 25% (Case 5), peak water levels occur about 1.5 and 2.5 days earlier than the observed data for stations east and west sides of the landfall, respectively. A higher forward speed storm propagates faster than the slower one. Due to the anticlockwise rotation of a hurricane on the northern hemisphere, winds on right side of the hurricane are enhanced by a higher forward speed and winds on the left side are weakened by the same. The peak water levels for nearshore stations (LA10, LA12, LC8a, LC9 and 8771341) are higher for increased forward speed than those for inland stations (LC6a, LF5 and LA9). On the contrary, when forward speed is decreased (Case 4), peak water levels occur 2.5 days later than the observed data for all stations east of the landfall. Notice that the peak arrival for faster forward speed is 1.5 days earlier, whereas that for slower speed is delayed by 2.5 days. The difference in the delay duration arises from the wind file time differences between these cases, explained in the second paragraph of Section 3.3. The peak water level for the station west of landfall occurs 1 day later than the observed data. The maximum water levels for inland stations (LC6a, LF5 and LA9) are higher than maximum water levels for the nearshore stations, since a slower storm has more time to push water overland, causing a high surge in the inland areas. A similar behavior was reported by Thomas et al. [19] for Hurricane Matthew, as mentioned earlier.

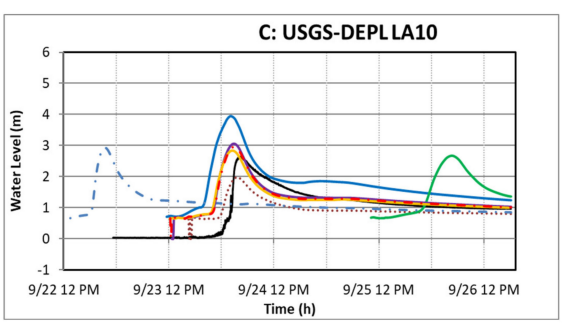

(a)

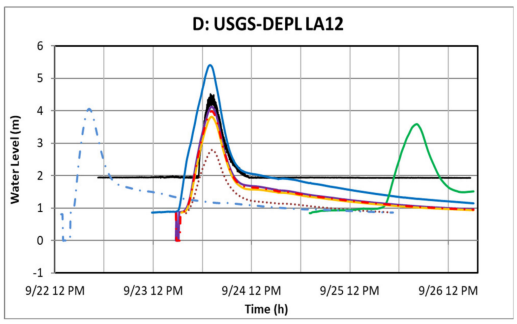

(b)

Figure 7. *Cont.*

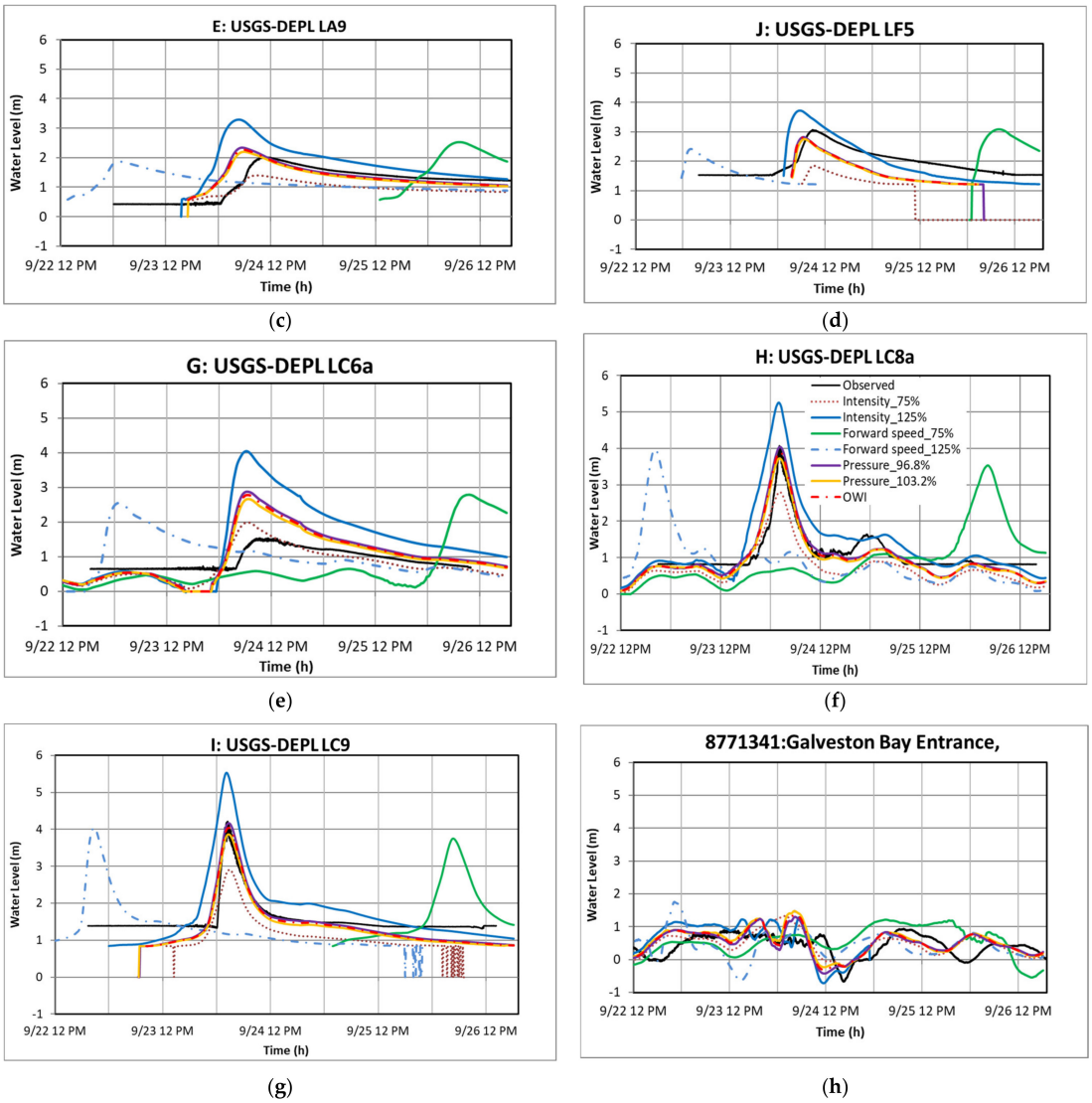

Figure 7. Effect of wind intensity, forward speed and surface pressure on storm surge variations with time using different meteorological forcing cases in Advanced CIRCulation and Simulating Waves Nearshore (ADCIRC + SWAN)—compared against station data collected during Hurricane Rita (9/22 12 p.m.–26 12 p.m.) for stations (**a**) USGS-DEPL LA10, (**b**) USGS-DEPL LA12, (**c**) USGS-DEPL LA9, (**d**) USGS-DEPL LF5, (**e**) USGS-DEPL LC6a, (**f**) USGS-DEPL LC8a, (**g**) USGS-DEPL LC9, (**h**) NOAA 8771341 (Nearshore).

When pressure is decreased to 96.8% (Case 6), surge levels are slightly higher than that of the base model (Case 1). However, when the pressure is increased to 103.2% (Case 7), the surge is slightly lower than Case 1. Since the wind intensity and forward speed remain the same for this pressure study, the resultant surge differences are only due to the incremental pressure changes.

4.3. Comparision of High Water Marks (HWMs)

A total of 144 USGS-observed High Water Marks (HWMs) are used to evaluate the performance of each modeled water level against the observed HWMs. Some of the HWMs and their locations with respect to the coast lines are shown in Figure 8a. Most of the high valued HWMs stations are near the coastline or in bay areas, and low valued HWMs stations are located inland. In Figure 8b–h, the red, yellow and light green points indicate over-prediction by the model by >1.5, 1.0~1.5 and 0.5~1.0 m, respectively. Similarly, blue, black and purple points indicate underprediction by the model by >1.5, 1.0~1.5 and 0.5~1.0 m, respectively. Green points indicate that observed and model HWMs match

within ±0.5 m. The black line represents the best fit line. Table 3 shows error statistics comparison of these simulated models. For the base case (Case 1) storm surge hindcast, 137 out of 144 stations are wet and the degree of determination (R^2) value is 0.704. The model overpredicts the high-water levels with Mean Normalized Bias (B_{MN}) of 0.203 and Root Mean Square Error (E_{RMS}) of 0.599.

Table 3. High Water Mark (HWM) Error Statistics for different cases.

Case	R^2	E_{RMS}	B_{MN}	Dry	Wet
Case 1 (Base or OWI)	0.704	0.599	0.203	7	137
Case 2	0.708	0.767	−0.221	10	134
Case 3	0.661	1.570	0.445	4	140
Case 4	0.691	0.441	0.038	9	135
Case 5	0.620	0.578	−0.003	9	135
Case 6	0.691	0.412	0.040	13	131
Case 7	0.717	0.398	−0.012	15	129

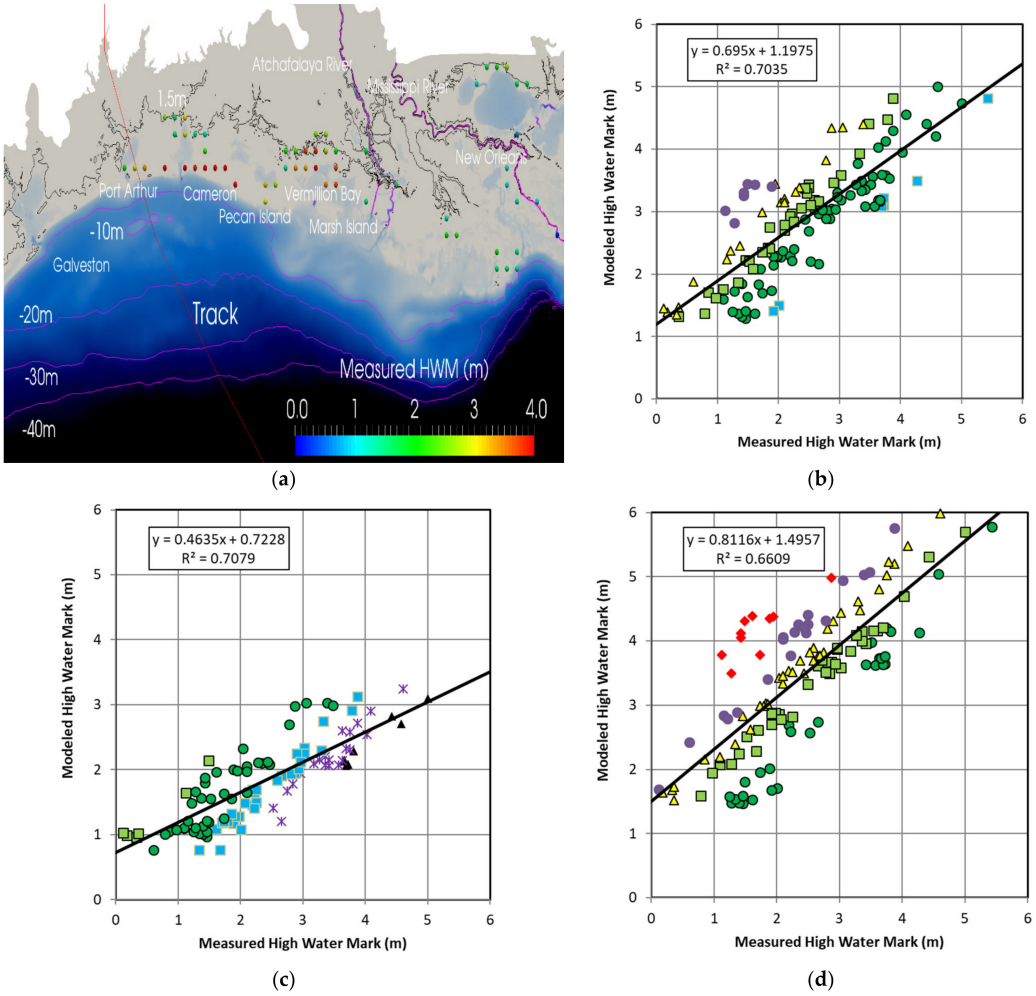

Figure 8. *Cont.*

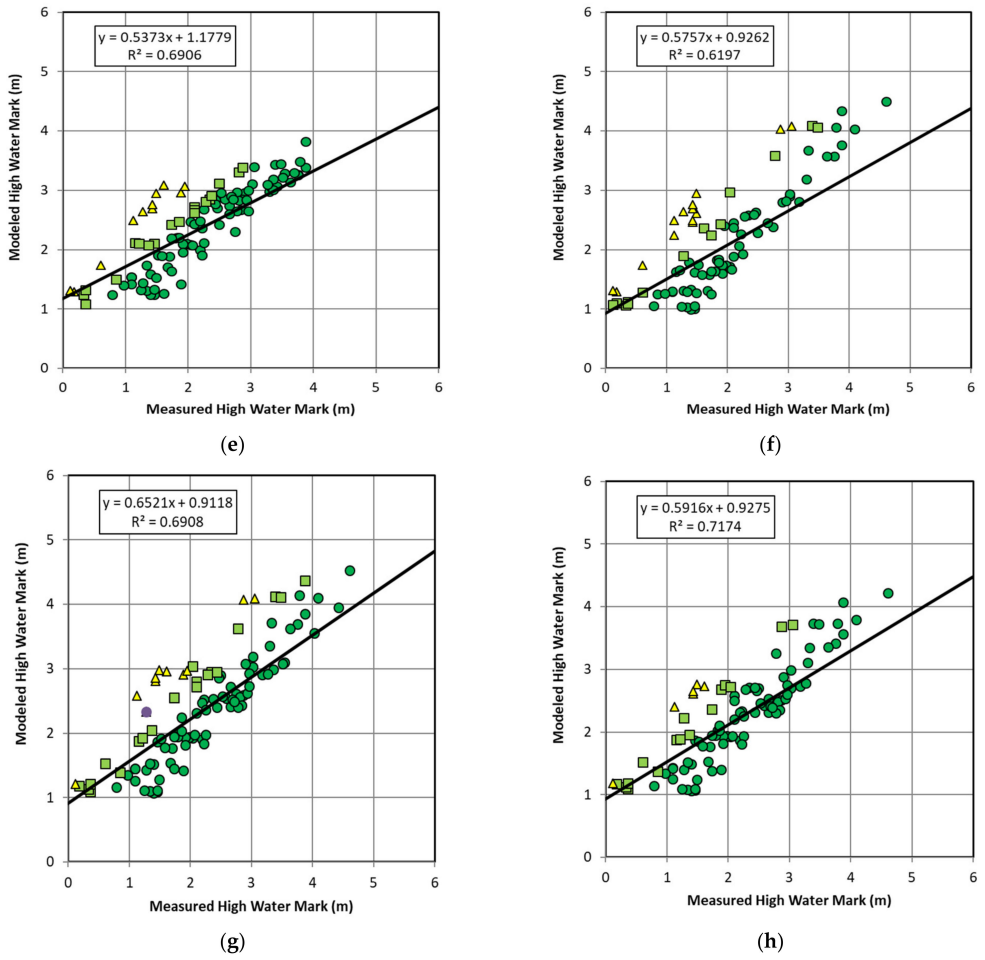

Figure 8. Scatter plots of observed HWMSs with those from ADCIRC+SWAN simulations using different meteorological forcings, (**a**) Measured HWMs on the map, (**b**) Case 1, (**c**) Case 2, (**d**) Case 3, (**e**) Case 4, (**f**) Case 5, (**g**) Case 6, (**h**) Case 7. Red, yellow, and light green points indicate over-prediction by the model by >1.5, 1.0~1.5 and 0.5~1.0 m, respectively. Blue, black and purple points indicate underprediction by the model by >1.5, 1.0~1.5 and 0.5~1.0 m, respectively. Dark green circles indicate a match within ±0.5 m. The black line represents the best fit line.

A comparison of Figure 8b,c reveals that the intercept of the best fit line is lower for Case 2 than that of Case 1, indicating an underprediction for HWMs stations with low surge values. The slope of the best fit line is lower for Case 2, which indicates an overall underprediction of high-surge valued HWMs stations as well. When wind intensity is decreased (Case 2), E_{RMS} increases with respect to that of Case 1 and the model underpredicts the HWMs. Although the ADCIRC+SWAN simulation wets fewer locations, the R^2 value obtained is slightly better than that from Case 1. On the contrary, increased wind intensity (Case 3) overpredicts the HWMs (compare Figure 8b,d) and has a much higher E_{RMS} value. The R^2 is lower than that of Case 1, with fewer dry stations. Variations in forward speed have lower values of E_{RMS} and lower R^2. Interestingly, the Mean Normalized Bias (B_{MN}) and Root Mean Square Error (E_{RMS}) for these cases are better than those of Case 1. In a slower storm (Case 4), the model slightly overpredicts the HWMs, while in a faster storm (Case 5), the model slightly underpredicts the HWMs, as indicated by signs and values of B_{MN}. Figure 8e,f intercept comparison reveals that a slower hurricane (Case 4) overpredicts stations with low HWMs, as those are located mostly inland. However, the stations with high HWMs are overpredicted by a faster hurricane (Case 5), as those are located near the open coast. Varying barometric pressure results in slightly worse correlations (R^2) between modeled and observed HWMs than Case 1. However, E_{RMS} and B_{MN} values are much smaller than those of Case 1, although there are more dry locations. Decreasing pressure

(Case 6) slightly overpredicts the HWMs, while increasing pressure (Case 7) slightly underpredicts the HWMs, as indicated by signs and values of B_{MN}. Figure 8g,h comparison reveals that the intercepts are about the same, but the slope of the best fit line is slightly higher for the lower pressure hurricane (Case 6), confirming its slight overprediction of surge for high HWMs stations.

4.4. Combined Effect of Wind Intensity and Forward Speed

The combined effect of wind intensity and forward speed is examined. As presented in Table 1, both wind intensity and forward speed are simultaneously increased and/or decreased in Cases 8–11.

Wind velocity vector plots at the time of landfall for these cases are similar to those of Figure 5 and are not repeated here for brevity.

As shown in Figure 9a, when both wind intensity and forward speed are decreased (Case 8), the storm surge decreases by more than 1.5 m. The opposite is observed when both parameters are increased (Case 9), as seen in Figure 9b. The impact of decreasing and increasing wind intensity and forward speed is more visible on the east side of landfall.

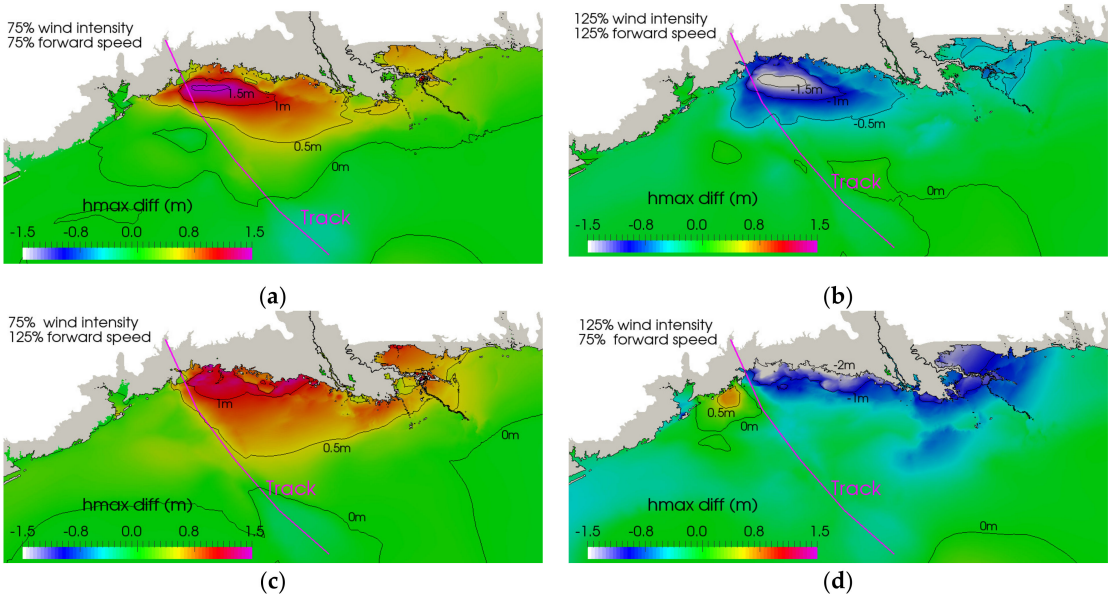

Figure 9. Departure of maximum water elevations from the base case (i.e., "hmax" of each simulation is subtracted from that of the base simulation); (**a**) Case 1, Case 8; (**b**) Case 1–Case 9; (**c**) Case 1, Case 10; (**d**) Case 1, Case 11.

Other experiments are conducted by simultaneously decreasing one factor while increasing the other. As shown in Figure 9c, when wind intensity decreases and forward speed increases (Case 10), the surge decreases in the nearshore by more than 1 m on the east side of landfall. However, when wind intensity increases and forward speed decreases (Case 11), as shown in Figure 9d, high intensity winds have more time to push water overland, which causes high and widespread flooding of more than 2 m in the inland areas on the east side of landfall. For Case 11, a decrease in flooding is observed on the west side of landfall. Overall, increasing wind intensity and decreasing forward speed simultaneously has the greatest effect on storm surge, since the hurricane has the strength and time to push the surge inland.

The ADCIRC+SWAN water level time series for the combined effect of wind intensity and forward speed are compared to the observed water levels at eight stations, as shown in Figure 10. When both wind intensity and forward speed are increased by 25% (Case 9), forward speed adds to the strength of the hurricane wind, especially on the right side of the hurricane. It is observed that storm surge impacts are different for inland and nearshore stations (i.e., LA10, LA12, LC8a and LC9) when compared with Case 3. For instance,

storm surge levels reduce by at least 0.3m on inland stations (i.e., LC6a, LF5 and LA9), while surge levels on nearshore stations increase by at least 0.3m. Additionally, the effect of increasing forward speed results in a 1.25 day earlier peak arrival than that of the base model (Case 1). The reverse happens when both wind intensity and forward speed are decreased by 25% (Case 8); the forward speed reduces the strength of the hurricane wind, especially on the right side. It is observed that storm surge levels increase by 0.3 m on inland stations, while surge levels on nearshore stations decrease by 0.3 m when compared with Case 2. This observation is consistent with earlier observations that a slower forward speed causes greater surge impacts in inland areas. The effect of decreasing forward speed results in a 2.08 day later peak arrival than that of the base model.

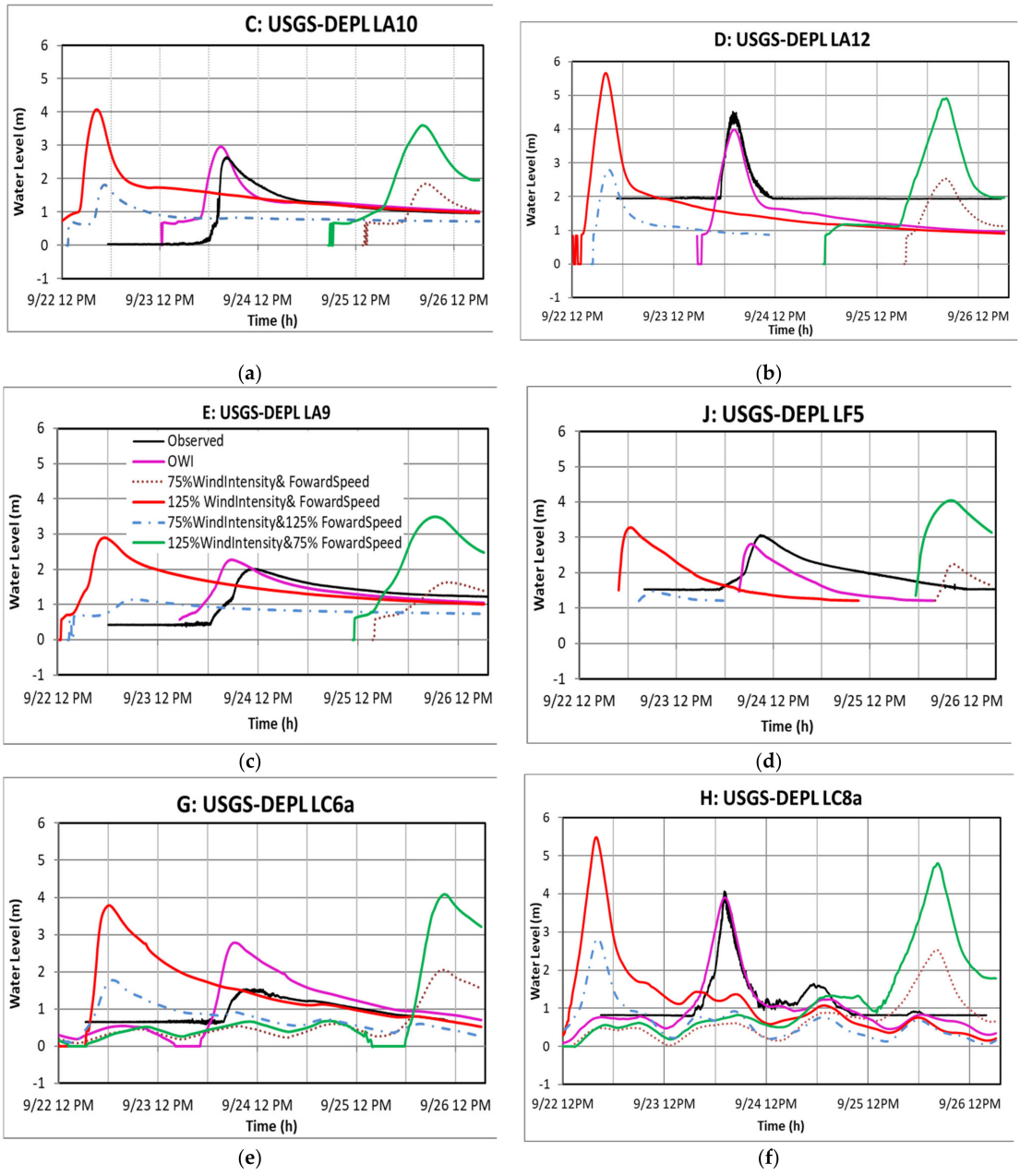

Figure 10. *Cont.*

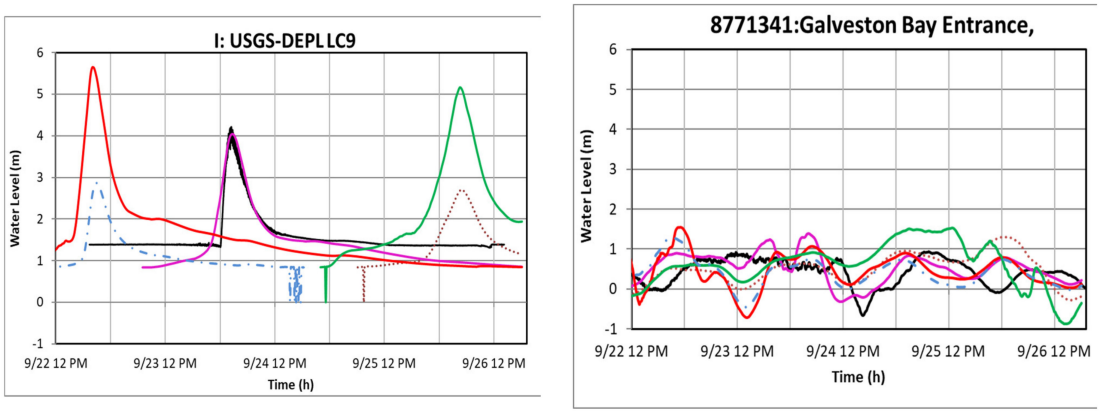

(**g**) (**h**)

Figure 10. Combined effect of wind intensity and forward speed on storm surge variations with time using different meteorological forcing cases in ADCIRC + SWAN, compared against station data collected during Hurricane Rita (9/22 12 p.m.–9/26 12 p.m.) for stations (**a**) USGS-DEPL LA10, (**b**) USGS-DEPL LA12, (**c**) USGS-DEPL LA9, (**d**) USGS-DEPL LF5, (**e**) USGS-DEPL LC6a, (**f**) USGS-DEPL LC8a, (**g**) USGS-DEPL LC9, (**h**) NOAA 8771341 (Nearshore).

Higher surges are observed when wind intensity is decreased but forward speed increased (Case 10) than when both are simultaneously decreased (Case 8) due to the additive effect of increased forward speed. The peak water levels of nearshore stations are lower compared to the case when both are simultaneously decreased, while at inland stations the storm surge is lower, since the storms are now moving faster and do not inundate the inland areas as much.

Increasing wind intensity and decreasing forward speed (Case 11) result in lower peak levels on nearshore stations than the case when both are simultaneously increased (Case 9) since reduced forward speed causes a subtractive effect. However, surge levels on inland stations (LC6a, LF5 and LA9) are observed to be higher than those in Case 9.

High Water Marks comparisons are done to study the combined effect of wind intensity and forward speed on surges. The simulated HWMs are compared for each of the simulations with measured HWMs. For brevity, the figures are not shown here, but the results are summarized in Table 4. All cases (Case 8–Case 11) have lower R^2 values than the base model (Case 1). When wind intensity and forward speed are decreased (Case 8), the model underpredicts and there are 37 dry stations. However, the model (Case 9) overpredicts when wind intensity and forward speed are increased and there are only five dry locations. Decreasing wind intensity and increasing forward speed (Case 10) cause underpredictions of the surge and there are 57 dry stations. Many inland stations remain dry as the wind is not strong enough, and water does not get enough time to travel far and wide. Increasing wind intensity and decreasing forward speed (Case 11) overpredicts the surge, although it has only four dry locations.

Table 4. HWM Error Statistics for wind intensity, forward speed, using Ocean Weather Inc. (OWI) meteorological forcing.

Case	R^2	E_{RMS}	B_{MN}	Dry	Wet
Case 1	0.704	0.599	0.203	7	137
Case 8	0.691	0.894	0.277	37	107
Case 9	0.621	1.16	0.315	5	139
Case 10	0.613	1.096	0.326	57	87
Case 11	0.605	1.53	0.427	4	140

5. Conclusions

A numerical experiment is performed to quantify storm surge responses to the varying wind intensity, forward speed and surface pressure of Hurricane Rita. The Interactive Objective Kinematic Analysis (IOKA) meteorological forcing is used as the base case to hindcast storm surges of Hurricane Rita using ADCIRC + SWAN. Various experimental simulations are conducted by manually varying each parameter, as well as examining the additive effect of wind intensity and forward speed on the storm surge. The findings are summarized below:

Wind intensity has the largest effect on storm surges, followed by the forward speed and surface pressure. A 25% change in wind intensity results in at least a 1 m change in storm surge. A 25% change in forward speed results in at least a 0.5 m change in storm surge, while a 3.2% change in pressure results in at least a 0.15 m change in storm surge.

Increasing wind intensity inadvertently increase the storm size and vice versa. The resultant storm surges are their combined effects.

The effect of varying forward speed depends on the geographical location of the hurricane. A faster storm causes high surges on the nearshore, but lower surges in inland areas such as in bays and rivers. A slower moving storm with more time to inundate inland areas causes high surges in bays and rivers, but lower surges on the nearshore.

The forward speed of the storm heavily influences the timing of peak water levels. Increasing forward speed by 25% advances the peak arrival by 1.25 days, while decreasing forward speed by 25% delays the peak arrival by 2.08 days.

Decreasing the center pressure by 30 millibars and decreasing the pressure field using Holland's rectangular hyperbola distribution increases the surge by approximately 0.67 cm per millibar, and vice versa. This effect is within 67% of a classical theoretical relationship (i.e., 1 cm surge change per millibar pressure). The discrepancy is probably due to the shallow water in gently sloped continental shelves near Rita landfall, and the uncoupled (or uninfluenced) wind field from pressure.

Wind intensity and forward speed have an additive effective on storm surge. The resultant effect depends on their combination, as can be predicted by individual effects summarized in items i through iv. The combined effect of increased wind intensity and decreased forward speed (Case 11) seems to increase surges the most, especially in inland areas, since the hurricane has the strength and time to push surges inland.

This study is specific to Hurricane Rita, and the findings should not be generalized. However, the findings stress the importance of the wind-driven component of storm surges on wide and gentle sloping continental shelves. They also demonstrate the importance of the additive effect of the wind intensity and forward speed on storm surge.

Author Contributions: A.M. performed all runs, post-processed results and provided analysis. M.K.A. designed the study, evaluated the analysis and provided technical feedback. All authors have read and agreed to the published version of the manuscript.

Funding: This research was funded by National Science Foundation—Excellence in Research, grant number 2000283 and the APC was funded by the same grant.

Institutional Review Board Statement: Not applicable.

Informed Consent Statement: Not applicable.

Acknowledgments: Authors are grateful to the University of North Carolina's Renaissance Computing Center for the access to their high-performance computing platform.

Conflicts of Interest: The authors declare sole responsibility of the research results.

References

1. Proudman, J. The propagation of tide and surge in an estuary. *Proc. R. Soc. Lond.* **1955**, *A231*, 8–24.
2. Proudman, J. Oscillations of tide and surge in an estuary of finite length. *J. Fluid Mech.* **1957**, *2*, 371–382. [CrossRef]
3. Prandle, D.; Wolf, J. Surge-Tide Interaction in the Southern North Sea. *Hydrodyn. Estuaries Fjords* **1978**, *23*, 161–185. [CrossRef]
4. Rossiter, J.R. Interaction Between Tide and Surge in the Thames. *Geophys. J. Int.* **1961**, *6*, 29–53. [CrossRef]

5. National Hurricane Center. Introduction to Storm Surge. 2019. Available online: https://www.nhc.noaa.gov/surge/surge_intro.pdf (accessed on 30 September 2019).
6. National Oceanic and Atmospheric Administration (NOAA). Hurricane Basics. May 1999. Available online: http://www.disastersrus.org/MyDisasters/NOAA/hurricanebook.pdf (accessed on 22 September 2020).
7. Lin, N.; Chavas, D. On hurricane parametric wind and applications in storm surge modeling. *J. Geophys. Res. Space Phys.* **2012**, *117*. [CrossRef]
8. Irish, J.L.; Resio, D.T. A hydrodynamics-based surge scale for hurricanes. *Ocean Eng.* **2010**, *37*, 69–81. [CrossRef]
9. Hope, M.E.; Westerink, J.J.; Kennedy, A.B.; Kerr, P.C.; Dietrich, J.C.; Dawson, C.N.; Bender, C.J.; Smith, J.M.; Jensen, R.E.; Zijlema, M.; et al. Hindcast and validation of Hurricane Ike (2008) waves, forerunner, and storm surge. *J. Geophys. Res. Ocean.* **2013**, *118*, 4424–4460. [CrossRef]
10. Kennedy, A.B.; Gravois, U.; Zachry, B.C.; Westerink, J.J.; Hope, M.E.; Dietrich, J.C.; Powell, M.D.; Cox, A.T.; Luettich, R.A., Jr.; Dean, R.G. Origin of the Hurricane Ike forerunner surge. *Geophys. Res. Lett.* **2011**, *38*, 1–5. [CrossRef]
11. Berg, R. *Tropical Cyclone Report Hurricane Ike 1–14 September 2008*; National Hurricane Center: Miami, FL, USA, 2009.
12. Irish, J.L.; Resio, D.T.; Ratcliff, J.J. The Influence of Storm Size on Hurricane Surge. *J. Phys. Oceanogr.* **2008**, *38*, 2003–2013. [CrossRef]
13. Luettich, R.A.; Westerink, J.J.; Scheffner, N.W. *ADCIRC: An Advanced Three-Dimensional Circulation Model for Shelves, Coasts and Estuaries; Report 1: Theory and Method-ology of ADCIRC-2DDI and ADCIRC-3DL*; Technical Report DRP-92-6; Department of the Army, USACE: Washington, DC, USA, 1991.
14. Westerink, J.J.; Luettich, R.A.; Blain, C.A.; Scheffner, N.W. *An Advanced Three-Dimensional Circulation Model for Shelves, Coasts and Estuaries; Report 2: Users' Manual for ADCIRC-2DDI*; Department of the Army, USACE: Washington, DC, USA, 1992.
15. Kolar, R.L.; Gray, W.G.; Westerink, J.; Luettich, R.A. Shallow water modeling in spherical coordinates: Equation formulation, numerical implementation, and application. *J. Hydraul. Res.* **1994**, *32*, 3–24. [CrossRef]
16. Rego, J.L.; Li, C. On the importance of the forward speed of hurricanes in storm surge forecasting: A numerical study. *Geophys. Res. Lett.* **2009**, *36*, 07609. [CrossRef]
17. Rego, J.L.; Li, C. Nonlinear terms in storm surge predictions: Effect of tide and shelf geometry with case study from Hurricane Rita. *J. Geophys. Res. Space Phys.* **2010**, *115*, 06020. [CrossRef]
18. Weisburg, R.H.; Zheng, L. Hurricane storm surge simulations for Tampa Bay. *Estuaries Coasts* **2006**, *29*, 899–913. [CrossRef]
19. Thomas, A.; Dietrich, J.C.; Asher, T.; Bell, M.; Blanton, B.; Copeland, J.; Cox, A.; Dawson, C.; Fleming, J.; Luettich, R. Influence of storm timing and forward speed on tides and storm surge during Hurricane Matthew. *Ocean Model.* **2019**, *137*, 1–19. [CrossRef]
20. Flather, R.A. Storm Surges. In *Encyclopedia of Ocean Sciences*; Steele, J., Thorpe, S., Turekian, K., Eds.; Academic: San Diego, CA, USA, 2001; pp. 2882–2892.
21. Sebastian, A.; Proft, J.; Dietrich, J.C.; Du, W.; Bedient, P.B.; Dawson, C.N. Characterizing hurricane storm surge behavior in Galveston Bay using the SWAN + ADCIRC model. *Coast. Eng.* **2014**, *88*, 171–181. [CrossRef]
22. Liu, Y.; Weisberg, R.H.; Zheng, L. Impacts of Hurricane Irma on the Circulation and Transport in Florida Bay and the Charlotte Harbor Estuary. *Chesap. Sci.* **2019**, *43*, 1194–1216. [CrossRef]
23. Kennedy, A.B.; Westerink, J.J.; Smith, J.M.; Hope, M.E.; Hartman, M.; Taflanidis, A.A.; Tanaka, S.; Westerink, H.; Cheung, K.F.; Smith, T.; et al. Tropical cyclone inundation potential on the Hawaiian Islands of Oahu and Kauai. *Ocean Model.* **2012**, *52*, 54–68. [CrossRef]
24. Joyce, B.R.; Gonzalez-Lopez, J.; Van Der Westhuysen, A.J.; Yang, D.; Pringle, W.J.; Westerink, J.J.; Cox, A.T. U.S. IOOS Coastal and Ocean Modeling Testbed: Hurricane-Induced Winds, Waves, and Surge for Deep Ocean, Reef-Fringed Islands in the Caribbean. *J. Geophys. Res. Oceans* **2019**, *124*, 2876–2907. [CrossRef]
25. Akbar, M.K.; Kanjanda, S.; Musinguzi, A. Effect of Bottom Friction, Wind Drag Coefficient, and Meteorological Forcing in Hindcast of Hurricane Rita Storm Surge Using SWAN + ADCIRC Model. *J. Mar. Sci. Eng.* **2017**, *5*, 38. [CrossRef]
26. Musinguzi, A.; Akbar, M.K.; Fleming, J.G.; Hargrove, S.K. Understanding Hurricane Storm Surge Generation and Propagation Using a Forecasting Model, Forecast Advisories and Best Track in a Wind Model, and Observed Data—Case Study Hurricane Rita. *J. Mar. Sci. Eng.* **2019**, *7*, 77. [CrossRef]
27. National Hurricane Center and Central Pacific Hurricane Center. Tropical Cyclone Climatology. May 1999. Available online: https://www.nhc.noaa.gov/climo/ (accessed on 22 September 2020).
28. Knabb, R.D.; Brown, D.P.; Rhome, J.R. *Tropical Cyclone Report, Hurricane Rita, 18–26 September 2005*; National Hurricane Center: Miami, FL, USA, 2006.
29. Kerr, P.C.; Donahue, A.S.; Westerink, J.J.; Luettich, R.A., Jr.; Zheng, L.Y.; Weisberg, R.H.; Roland, A. US IOOS coastal and ocean modeling testbed: Inter-model evaluation of tides, waves, and hurricane surge in the Gulf of Mexico. *J. Geophys. Res. Ocean.* **2013**, *118*, 5129–5172. [CrossRef]
30. Mukai, A.; Westerink, J.; Luettich, R., Jr.; Mark, D. *Eastcoast 2001, a Tidal Constituent Database for Western North Atlantic, Gulf of Mexico, and Caribbean Sea*; Tech. Rep. ERDC/CHL TR-02-24; US Army Eng. Res. and Dev. Cent., Coastal and Hydraulics Lab.: Vicksburg, MS, USA, 2002; p. 201.
31. SWAN—Scientific and Technical Documentation Version 40.91AB. 2013. Delft University of Technology, Environmental Fluid Mechanics Section. 15 July 2017. Available online: http://www.swan.tudelft.nl (accessed on 8 August 2020).

32. Luettich, R.A., Jr.; Westerink, J.J. *Implementation of the Wave Radiation Stress Gradient as a Forcing for the ADCIRC Hydrodynamic Model: Upgrades and Documentation for ADCIRC Version 34.12*; Contractors Report; Department of the Army, US Army Corps of Engineers, Waterways Experiment Station: Vicksburg, MS, USA, May 1999; p. 9.
33. Cox, A.T.; Greenwood, J.A.; Cardone, V.J.; Swail, V.R. An interactive objective kinematic analysis system. In Proceedings of the Fourth International Workshop on Wave Hindcasting and Forecasting, Banff, AB, Canada, 16–20 October 1995; pp. 109–118.
34. Cardone, V.J.; Cox, A.T. Tropical cyclone wind field forcing for surge models: Critical issues and sensitivities. *Nat. Hazards* **2009**, *51*, 29–47. [CrossRef]
35. Holland, G.J.; Belanger, J.I.; Fritz, A. A Revised Model for Radial Profiles of Hurricane Winds. *Mon. Weather. Rev.* **2010**, *138*, 4393–4401. [CrossRef]
36. Gao, J.; Luettich, R.; Fleming, J. Development and initial evaluation of a generalized asymmetric tropical cyclone vortex model in ADCIRC. In Proceedings of the ADCIRC Users Group Meeting, Vicksburg, MS, USA, 29–30 April 2013; Volume 16.
37. Harris, D.L. *Characteristics of the Hurricane Storm Surge (No. 48)*; Department of Commerce, Weather Bureau: Washington, DC, USA, 1963.